Considering The Remaining Useful Life Of Lithium Batteries For Modern Tram Power System Capacity Configuration

Fengyang Gao[1], Fengxu Qi[1*], Guopeng Han[2], Jia Liu[1], and Qingyin Liu[1]

[1] College of Automation and Electrical Engineering, Lanzhou jiaotong University, Lanzhou 730070 China
[2] CRRC Tangshan Co., Ltd., Tangshan 063035 China
[*] Corresponding author. E-mail: 472926645@qq.com

Received: Jul. 16, 2023; Accepted: Oct. 21, 2024

Configuring trams with hybrid power systems of appropriate capacity can effectively improve the operational efficiency of trams. The traditional capacity configuration depends on the engineering experience, which leads to the problem of high configuration cost. In this paper, based on the remaining useful life (RUL) prediction of lithium batteries, a capacity configuration method of tramway hybrid power system considering lithium battery RUL is proposed. Prediction of lithium battery RUL based on particle filtering (PF) algorithm and comparative analysis with extended kalman filter (EKF) algorithm. Analyzing the cost structure of the power system, constructing a system capacity configuration model, including objective function, constraints, and solving the model by using honey badger algorithm (HBA). Finally, the calculation example compares and analyzes the impact of different energy storage methods on the total annual average minimum cost of the system to verify the feasibility of the proposed method. The results show that the total annual average minimum cost of hybrid energy storage is only 14.603 million yuan, which decreases by 38.2% compared with the single-type battery energy storage capacity configuration, and greatly improves the system economy.

Keywords: modern tramway; hybrid power system; lifetime prediction; particle filter; capacity configuration

http://dx.doi.org/10.6180/jase.202509_28(9).0006

1. Introduction

Lithium battery/fuel cell/supercapacitor hybrid system tramways have the advantages of fast speed, environmental protection and energy saving, and comfortable ride. However, lithium batteries have high production costs, poor safety, and are prone to fire, explosion and other hazards in case of impact [1], and over-charging and over-discharging of lithium batteries will lead to durability degradation [2], thus reducing the overall life of the power system. By predicting the remaining useful life (RUL) of lithium batteries and rationally configuring the power system capacity, the economy, reliability and safety of the power system can be significantly improved.

At present, commonly used lithium battery life prediction methods mainly include extended kalman filter (EKF), unscented kalman filtering (AUKF) and particle filtering (PF). [3] put forward a method to predict lithium battery RUL by combining the double exponential degradation model with EKF, but the prediction accuracy is low and there is a certain prediction error. [4] uses AUKF based on weight optimization to estimate the state of charge of lithium batteries, which solves the problem of inaccurate prediction results caused by cumulative errors, but the method needs to linearize the nonlinear function expansion, which increases the amount of computation. However, PF algorithm has a good ability to deal with nonlinear problems in dynamic systems [5], and is an ideal state tracking and prediction method for state estimation and life prediction of lithium batteries [6]. [7] introduces PF algorithm in lithium battery health state estimation and fault diagnosis, which realizes accurate prediction of lithium

battery health state and uncertainty estimation of RUL, and reduces the amount of computation. [8] aiming at the problem of poor long-term life prediction of lithium batteries, the uncertainty expression of lithium battery RUL prediction is obtained by deriving the posterior probabilistic relationship between the lithium battery life and the capacity observations in the PF algorithm, which reduces the prediction error.

On the basis of lithium battery RUL prediction, rational configuration of capacity is an important factor to ensure the economic and reliable operation of the system [9]. There are two main methods commonly used for hybrid power system capacity configuration, one is to establish the objective function with the optimal capacity of the energy storage device. [10] proposes a capacity optimization allocation strategy for energy storage equipment under fault disturbance scenarios, and by controlling the influence of differential and proportional coefficients on the capacity of the energy storage equipment, the calculation method of the optimal capacity of the energy storage equipment is obtained, but the calculation is more complicated. [11] constructs the optimal configuration scheme of energy storage equipment based on the specific needs of thermal replacement capacity and load supply capacity of wind farms, which is simple and easy to implement, but fails to take into account the impact of the current higher cost of energy storage on the economy of the energy storage system. The second is to establish an objective function in terms of cost minimization. [12] configures the energy storage capacity with the optimization objective of lowest total annual cost, but fails to take into account the costs incurred in investing in, replacing, and maintaining the equipment over its entire life cycle. [13] constructs a combined operation system, and puts forward the capacity optimization with the lowest cost and the smallest carbon emission as the optimization goal, which allocates carbon emission but does not consider the whole life of the system caused by battery pack loss. In summary, [3, 4] and [7, 8] only perform RUL prediction or state estimation for lithium battery systems, while [10-13] only perform capacity configuration for systems, neither of which combine lithium battery RUL prediction and system capacity configuration. Therefore, how to improve the prediction accuracy of lithium battery RUL and improve the power system economy through reasonable capacity configuration will become a major challenge.

To address the above problems in the existing research, a method for capacity allocation of hybrid power system for streetcars considering lithium battery RUL is proposed, with the main contributions as follows:

1. Utilizing the particle filtering algorithm to effectively predict the remaining service life of lithium batteries reduces the amount of computation and has a higher prediction accuracy compared with the extended Kalman filtering algorithm.

2. By predicting the remaining service life of the lithium battery in the early stage, it provides a prerequisite for the later capacity configuration, thus reducing the cost of the hybrid system and improving the system economy.

3. Dividing the power system cost into three categories, namely, initial investment cost, component replacement cost, and operation and maintenance cost, is more practical than the costing method that only considers one-time investment.

4. This paper is organized as follows: section 2 introduces the hybrid system components, including lithium battery model, fuel cell model and supercapacitor model. Section 3 introduces the RUL prediction method based on PF, including the principle of PF, capacity decline analysis of lithium batteries, capacity degradation model of lithium batteries, analysis of RUL prediction results based on PF and comparison of prediction results between PF and EKF. Section 4 constructs the power system capacity allocation model including objective function, constraints and solves the model by using honey badger algorithm (HBA). Section 5 is an example analysis, including parameter setting, optimization algorithm validity verification, capacity configuration results and capacity configuration results comparative analysis. Section 6 is the conclusion and prospect of this paper.

2. Hybrid system structure

The modern tram hybrid power system composed of Lithium battery/fuel cell/supercapacitor is shown in Appendix A, Fig.A1, and the power source is composed of Lithium battery, fuel cell and supercapacitor. Within, lithium batteries and fuel cells are connected to the DC bus through bi-directional and uni-directional DC/DC converters to provide the power required by the load, while the supercapacitor plays the role of “peak shaving and valley filling”.

2.1. Lithium battery improvement model

Lithium batteries uses a modified Shepherd curve fitting model [14]. The addition of a voltage polarization term to the battery discharge voltage expression allows for a better characterization of the effect of battery state of charge on

battery performance. In addition, to ensure stability, the model uses the filtered battery current instead of the actual battery current to calculate the polarization resistance.

The lithium battery terminal voltage can be expressed as Eq. (1) [14]

$$V_{\text{batt}} = E_0 - C \cdot \frac{Q}{Q - it} \cdot it - R_{\text{b}} \cdot i + A_{\text{b}} \exp(-B \cdot it) - C \cdot \frac{Q}{Q - it} \cdot i^* \quad (1)$$

Where, E_0 is the lithium battery constant voltage; C is the polarization constant; Q is the lithium battery capacity; i^* is the filtered lithium battery current; it is the actual lithium battery charge; A_{b} is the amplitude of the index area; B is the inverse of the time constant of the index area; R_{b} is the lithium battery internal resistance; $C \cdot [Q/Q\text{-it}\,] \cdot it$ is the polarization voltage; $C \cdot [Q/Q - it]$ is the polarization resistance (Pol_{res}).

During the charging process, the battery voltage suddenly increases after filling, and this behavior is expressed by modifying the polarization resistance (only during charging) as:

$$Pol_{\text{res}} = C \cdot \frac{Q}{it - 0.1 \cdot Q} \quad (2)$$

2.2. Fuel cell model

The fuel cell uses a semi-empirical steady state model [15]. In the ideal case, the output voltage is:

$$U_{\text{cell}} = E_{\text{Nemst}} - U_{\text{act}} - U_{\text{ohm}} - U_{\text{con}} \quad (3)$$

Where, E_{Nernst} is the thermodynamic electric potential; U_{act} is the activation polarization overvoltage; U_{ohm} is the ohmic polarization overvoltage; U_{con} is the concentration polarization overvoltage.

Within, the activated polarization overvoltage is expressed as:

$$U_{\text{act}} = -[\xi_1 + \xi_2 T + \xi_3 T \ln(C_{O2}) + \xi_4 T \ln(I)] \quad (4)$$

Where, $\xi_1, \xi_2, \xi_3, \xi_4$ are empirical factors; T denotes the internal temperature of the fuel cell; C_{O2} denotes the dissolved oxygen concentration at the cathode gas-liquid interface in mol/cm^3; and I is the actual current density of the fuel cell.

The ohmic polarization overvoltage can be expressed as:

$$U_{\text{obm}} = IR_{\text{cell}} \quad (5)$$

Where, R_{cell} is the equivalent internal resistance.

Differential polarization overvoltage is expressed as:

$$U_{\text{con}} = -B' \ln\left(1 - \frac{I}{I_{\text{max}}}\right) \quad (6)$$

Where, B' is the system parameter; and I_{max} represents the maximum current density of the fuel cell.

2.3. Supercapacitor model

Supercapacitors uses the Stern model, which combines the Helmholtz and Gouy-Chapman models [16]. Considering the resistive losses, the supercapacitor output voltage is expressed as:

$$V_{\text{SC}} = \frac{Q_{\text{T}}}{C_{\text{T}}} - R_{\text{SC}} \cdot i_{\text{SC}} \quad (7)$$

Within,

$$Q_{\text{T}} = \int i_{\text{SC}}\, \text{d}t \quad (8)$$

$$C_{\text{T}} = \frac{N_{\text{P}}}{N_{\text{S}}} \cdot C \quad (9)$$

Where, C_{T} is the capacitance value of the supercapacitor composed of N_{S} monomers in series and N_{p} monomers in parallel; Q_{T} is the total electric charge; R_{SC} and i_{SC} are the equivalent internal resistance and transient current of the supercapacitor, respectively.

3. Rul prediction method based on particle filtering

3.1. PF algorithm

The core idea is to approximate the probability density function of a systematic random variable with some discrete random sampling points, replacing the integral operation with the sample mean to obtain the minimum variance estimate of the state [17].

The state space model of the algorithm is as follows:

$$\begin{cases} x_k = f(x_{k-1}) + v_k \\ y_k = h(x_k) + w_k \end{cases} \quad (10)$$

Within, x_k denotes the state value of the system at the current moment, and y_k indicates the observed value of the system at the current moment. v_k and w_k represent the system noise and observation noise, respectively. $f(\bullet)$ is the state equation, which denotes the functional relationship between the state of the system at the previous moment and at the current moment; and $h(\bullet)$ is the observation equation, which denotes the functional relationship between the state of the system and the observation value.

The methodology includes the following steps:

1. Particle initialization [18].

2. Importance sampling [18]. The distribution of importance is as follows:

$$q\left(x_k \mid Y_k\right) \approx \sum_{i=1}^{N} \delta\left(x_k - x_k^i\right) \tag{11}$$

Where, $\delta(\bullet)$ is a $0-1$ variable function.

3. Calculate particle weights $\omega_k^{(i)}$:

$$\omega_k^{(i)} = \frac{p\left(x_k^{(i)} \mid Y_k\right)}{q\left(x_k^{(i)} \mid Y_k\right)} \tag{12}$$

4. Standardization. Standardize the obtained weights:

$$\omega_k^{(i)} = \frac{\omega_k^{(i)}}{\sum_{i=1}^{N} \omega_k^{(i)}} \tag{13}$$

5. Resampling [19]. The degree of particle degradation can be estimated by the following formula:

$$N_{\text{eff}} = \frac{1}{\sum_{i=1}^{N}\left[\omega_k^{(i)}\right]^2} \tag{14}$$

Where, N_{eff} represents the effective number of particles. The lower the N_{eff} is, the more serious the particle degradation is, and the more resampling should be performed. Usually, a threshold N_{th} can be set in advance, and when $N_{\text{eff}} \leq N_{\text{th}}$, resampling is required.

6. Power estimation. Through the above steps, if the cycle ends then the value of k is the estimated value of the battery RUL.

$$\bar{x}_k = \sum_{i=1}^{N} \omega_k^{(i)} x_k^{(i)} \tag{15}$$

3.2. Lithium battery capacity decline analysis

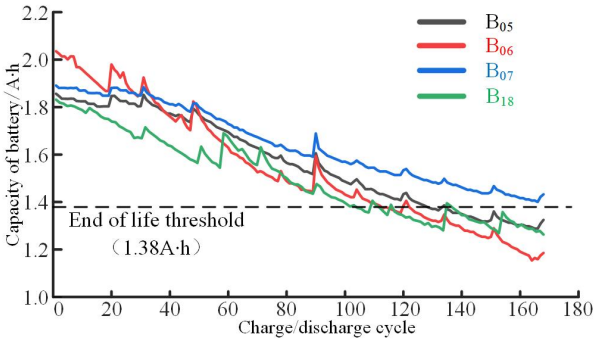

Fig. 1. Battery capacity degradation curve.

According to the lithium battery capacity formula:

$$Q = \int_{t_c}^{t_d} I(t)\mathrm{d}t \tag{16}$$

Where, t_c denotes the time when lithium battery is fully charged; t_d represents the time when lithium battery is fully discharged; Q signifies the lithium battery capacity.

The original experimental data used for lithium battery capacity degradation was obtained from the open source battery dataset of NASA Prognostics Center of Excellence (PCoE), which contains four sets of charge/discharge experimental data. Four sets of data for the same type of battery were extracted from the original test set as B_{05}, B_{06}, B_{07} and B_{18}. Then the four groups of lithium battery capacity data were exponentially fitted, and the change curves of four groups of lithium battery capacity with charging and discharging cycles were obtained as shown in Fig. 1. It can be seen from Fig. 1, with the increase in the number of charging and discharging times, the capacity of lithium batteries gradually decreased, that is, the remaining service life of lithium batteries is gradually shortened, and the capacity of the battery and the number of charging and discharging times is a non-linear relationship.

3.3. Lithium battery capacity degradation model

The empirical model of capacity recession is a key factor governing the prediction accuracy of RUL for lithium batteries, and the empirical models mainly include linear and exponential models [20], within which the most commonly used is the exponential model. Since the capacity degradation of lithium batteries is a complex electrochemical process, a suitable model is needed to fulfill the requirements of the nonlinear trend characteristics of battery capacity degradation. Combined with the equivalent circuit model of lithium batteries, it is found that the double-exponential empirical degradation model can accurately characterize the actual capacity degradation trend of the batteries, and its use of two exponential forms of the structure has better applicability for nonlinear features [21]. Therefore, the double-exponential empirical degradation model is chosen for subsequent analysis in this paper.

The battery capacity decay obeys Eq. (17):

$$Q = a * \exp(b * k) + c * \exp(d * k) \tag{17}$$

Where, k is the number of cycles; a, b, c, d are the model parameters and are all related to the lithium battery itself, within which a and c denote the lithium battery internal impedance, and b and d represent the lithium battery degradation rate, so that when a, b, c, d are estimated more accurately, then the simulation of the lithium battery itself will be more realistic, and the more accurately the lithium battery life can be predicted.

According to Fig. 1, the data set of lithium battery B_{07} will be removed from the subsequent analysis because the downward trend of lithium batteries B_{05}, B_{06}, and B_{18} is more pronounced compared to lithium battery B_{07} and lithium battery B_{07} has not reached the set end of life threshold. In the PF algorithm, the lifetime threshold of the lithium battery is set to 1.38 A · h, and the number of particles is set to 200 . When the lithium battery capacity is less than 1.38 A · h, it is considered that the lifetime of the battery pack in this batch is exhausted, and it is necessary to replace the battery pack.

3.4. Analysis of RUL prediction results based on PF algorithm

The prediction curve is built based on the measured data of lithium battery capacity from NASA PCoE and predicts how many more cycles the lithium battery will fail. Before proceeding with the particle filtering algorithm, it is necessary to determine the state initial values. a, b, c, and d initial values can be fitted by the MATLAB curve fitting toolbox for the first n data, and the state initial values are generally taken as the average of each state parameter, that is:

$$[a_0, b_0, c_0, d_0]^{\mathrm{T}} = [1.802, -0.00373, 0.1065, -0.006758]^{\mathrm{T}}$$

The PF algorithm is implemented through the MATLAB simulation platform, and the initial degradation model is obtained by substituting the initial values into Eq. (17). In order to verify the validity of the proposed method, the algorithm flow in Section 3.1 and the empirical model in Section 3.3 are used as indicators, respectively, and the prediction start time is selected to be the 50th, 70th, and 90th cycles, and the PF algorithm is used to predict the RUL of lithium batteries. The remaining life prediction curve and tracking error curve of the lithium battery B18 are obtained as shown in Fig. 2.

In Fig. 2(a)(b)(c), the capacity curve before the prediction point, the capacity prediction curve, and the actual lithium battery decline curve are given, respectively. Within which the horizontal coordinate represents the charge/discharge cycle and the vertical coordinate represents the battery capacity, the red curve is the filtered estimate obtained from the particle filter prediction, the blue curve is the experimental measurement data of lithium battery B_{18}, the yellow line is the prediction starting point from the yellow line, and the green curve is the result obtained from the prediction based on the value of the cyclic cycle without any processing. It can be seen that the PF algorithm has good tracking ability. Before the prediction start point, the PF algorithm mainly gets the values of a, b, c and d after filtering based on the observation data of Q. After the prediction start point, the values of a, b, c and d are obtained by utilizing the pre-filtering to predict the RUL of the lithium battery.

Fig. 2(a) illustrates the prediction results for the first 50 cycles. After 50 cycles, the prediction algorithm is executed, and every time a capacity value is output, it is judged whether the failure threshold is reached; if the failure threshold is reached, the iteration is stopped and the number of cycles at the end of the iteration is output; if the failure threshold is not reached, the iterative algorithm is continued. It can be seen that the RUL prediction of lithium battery based on the PF algorithm results in a 136 cycles, while the true end of life point is 129 cycles, with an error of 5.43%; Fig. 2(b) shows the prediction results for the data of the first 70 cycles, and the lithium battery RUL prediction based on the PF algorithm is 125 cycles with an error of 3.10%; similarly, the prediction results for 90 cycles are shown in Fig. 2(c), and the PF method predicts 131 cycles with 1.56% error, as shown in Table 1. As can be seen, the RUL prediction results based on the PF algorithm are more accurate as the prediction point period increases, and the prediction results match the true life values of the lithium battery data used in NASA PCoE.

In Table 1, RUL start / cycle denotes the cycle where the prediction starts; $\mathrm{RUL_{real}}$ / cycle denotes the true end of life point of the battery data used; $\mathrm{RUL_{pred}}$ / cycle denotes the predicted value of the remaining useful life of the lithium battery; err/cycle denotes the prediction error; and $\mathrm{RUL_{err}}$/% denotes the absolute prediction error.

Fig. 2(d) shows the error curve between the data predicted based on the PF algorithm and the experimental data. As can be seen from Fig. 2(d), the error between the data predicted based on the PF algorithm and the experimental data is small in the whole cycle, and its error value is kept around 0.05, which is near the horizontal line and the error change is small, and it has good stability.

3.5. Comparison of PF and EKF prediction results

EKF is a common algorithm for lithium battery RUL prediction. In order to further verify the validity of the proposed method, the same lithium battery data are used, and the start time of the prediction is selected as the 70th cycle, and the EKF algorithm is applied to predict the RUL of the lithium battery, Fig. 3 shows the EKF prediction curve with the start time of the prediction as the 70th cycle, and Table 2 shows the comparison results of the two prediction methods. As can be seen in Fig. 3, the EKF based prediction deviates more from the true value and the prediction is

Table 1. RUL prediction results for lithium batteries.

RUL_{start} / cycle	RUL_{real} / cycle	RUL_{pred} / cycle	err/cycle	RUL_{err} /%
50	129	136	7	5.43
70	129	125	4	3.10
90	129	131	2	1.56

Table 2. Comparison of prediction results.

Methods	70 cycles			
	RULrea/cycle	RUL_{pred} /cycle	err/cycle	RULerr/%
PF	129	125	4	3.10
EKF	129	139	10	7.75

less effective. From Table 2, it can be seen that at the 70th cycle of the same prediction starting point, the PF method predicts the RUL of lithium batteries for 125 cycles, with an absolute error of prediction error of 3.10%. The prediction result of lithium battery RUL obtained by the EKF method is 139 cycles with a prediction error of 7.75%, and the prediction accuracy based on the PF algorithm is higher than the prediction accuracy of the EKF algorithm.

4. Power system capacity configuration program

The traditional capacity configuration is not highly accurate due to the reliance on engineering experience, so it is necessary to consider the remaining useful life of lithium batteries in the power system capacity configuration model, and provide prerequisites for the later capacity configuration by predicting the remaining service life of lithium batteries in the early stage, so as to improve the accuracy of the capacity configuration.

4.1. Objective function

The costs incurred in their operation need to be considered when making capacity allocations. Therefore, a capacity allocation model for power system operating economics was developed. Since battery power systems are devices that are used over a long period of time and require regular post-maintenance, the costs are calculated in the following three ways.

1. Initial investment cost.

$$C_1 = m_{cp}P_{cap} + m_{cc}C_{cap} + m_{bp}P_{bat} + m_{bc}C_{bat} \quad (18)$$

Where, P_{cap} , P_{bat} are the rated power of the supercapacitor and battery, C_{cap} , C_{bat} are the rated capacity of the supercapacitor and battery; m_{cp}, m_{cc} are the power unit price and capacity unit price of the supercapacitor, m_{bp}, m_{bc} are the power unit price and capacity unit price of the battery.

2. Component replacement costs.

$$C_2 = n_{cap}\left(m_{bp}P_{bat} + m_{bc}C_{bat}\right) + n_{bat}\left(m_{cp}P_{cap} + m_{cc}C_{cap}\right) \quad (19)$$

Where, n_{cap} and n_{bat} are the number of times the supercapacitor and battery are replaced throughout the operation, respectively.

3. Operation and maintenance costs.

$$C_3 = T_{act}\left(u_{cap}\,C_{cap} + u_{bat}\,C_{bat}\right) \quad (20)$$

Where, T_{act} is the actual operating life of the power system; u_{cap} and u_{bat} are the unit price for operation and maintenance of the supercapacitor and battery, respectively.

In summary, the average annual minimum cost is:

$$C_{min} = \left[\left(C_1 + C_2 + C_3\right)/T_{act}\right] \quad (21)$$

4.2. Constraints

1. SOC constraints.

$$\begin{cases} SOC_{bat\text{-}min} \le SOC_{bat}(t) \le SOC_{bat\text{-}max} \\ SOC_{cap\text{-}min} \le SOC_{cap}(t) \le SOC_{cap\text{-}max} \end{cases} \quad (22)$$

Where, $SOC_{bat\text{-}max}$, $SOC_{bat\text{-}min}$ are the upper and lower limits of state of charge of the battery; $SOC_{cap\text{-}max}$, $SOC_{cap\text{-}min}$ are the upper and lower limits of state of charge of the supercapacitor; $SOC_{bat}(t)$ and $SOC_{cap}(t)$ are state of charge of the battery and the supercapacitor at time t.

2. Power balance constraints. The output power of the batteries and supercapacitors should be less than or equal to the rated power of the system $P_{out}(t)$.

$$\begin{cases} P_{bat}(t) + P_{cap}(t) \le P_{out}(t) \\ P_{out}(t) \ge 0 \\ -P_{bat\text{-}max} \le P_{bat}(t) \le P_{bat\text{-}max} \\ -P_{cap\text{-}max} \le P_{cap}(t) \le P_{cap\text{-}max} \end{cases} \quad (23)$$

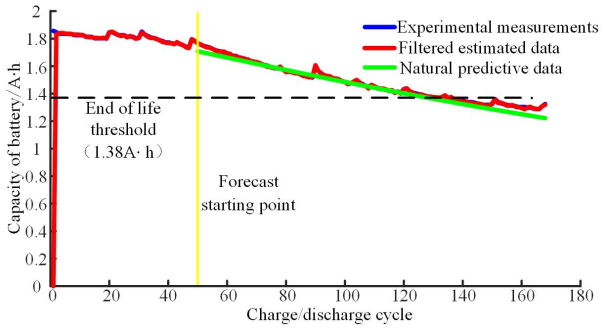

(a) Forecast results for 50 cycles.

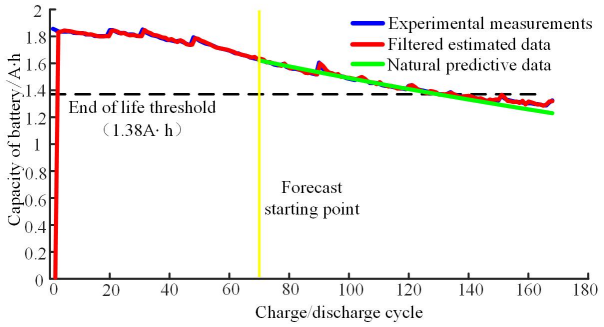

(b) Forecast results for 70 cycles.

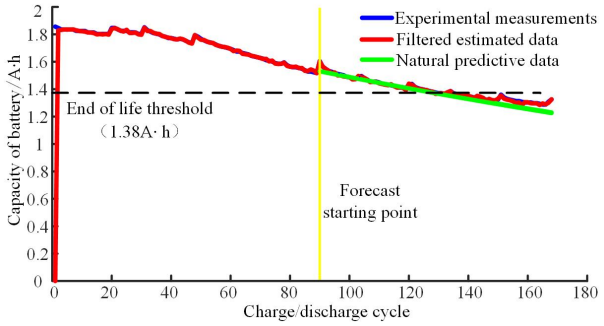

(c) Forecast results for 90 cycles.

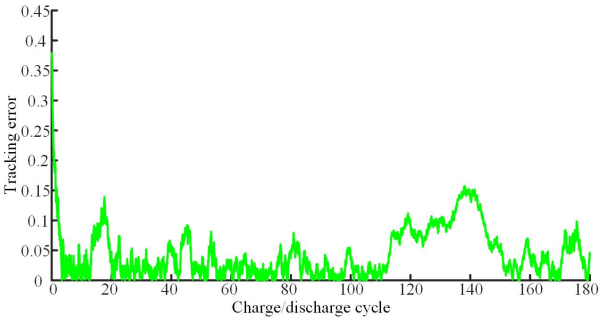

(d) Tracking error curve.

Fig. 2. Forecast result and tracking error curve.

3. Charge/discharge conservation constraints.

$$\sum_{k=1}^{i} P_{\text{ch}}(k) = \sum_{k=1}^{i} P_{\text{disch}}(k) \tag{24}$$

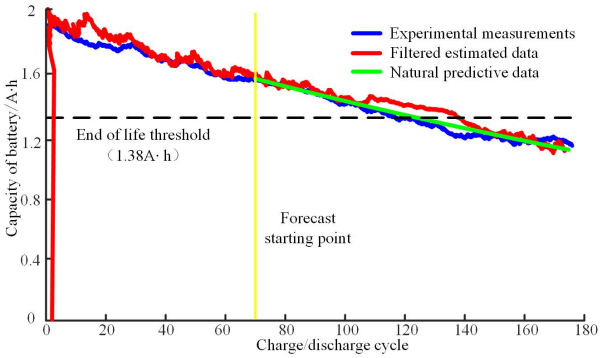

Fig. 3. EKF forecast: 70 cycles.

Where, P_{ch} and P_{disch} are the charging power and discharging power of the power system, respectively; k is the number of cycles.

4.3. Honey badger algorithm

HBA has fast convergence, high accuracy and strong search capability [22], which is used to optimize the objective function of the dynamical system, and the optimization process is as follows:

Step 1: Population initialization. Assuming that the population size is N and the problem dimension is D, the initialization formula is as follows:

$$x_{ij} = lb_j + r_1 \cdot \left(ub_j - lb_j\right) \tag{25}$$

Within which $i = 1, 2, \ldots, N; j = 1, 2 \ldots, D.x_{ij}$ denotes the j th dimensional variable of individual i, ub_j and lb_j denote the upper and lower bounds of the j th dimensional variable, respectively, and r_1 is a random number between $[0, 1]$.

Step 2: Define the odor intensity (O).

$$\begin{cases} O_i = r_2 \times \frac{S}{4\pi d_i^2} \\ S = (x_i - x_{i+1})^2 \\ d_i = x_{\text{prey}} - x_i \end{cases} \tag{26}$$

Within which S is the concentration intensity, d_i is the distance between the prey and the i th honey badger, r_2 is a random number between $[0, 1]$, and x_{prey} represents the optimal individual in the population, the prey.

Step 3: Update the density factor (α).

$$\alpha = C \times \mathrm{e}^{-\frac{t}{T_{\max}}} \tag{27}$$

Within this, $T_{\max}$ is the maximum number of iterations, t is the current number of iterations, and C is a constant not less than 1 , usually set to 2 .

Step 4: Update individual locations. Specifically, it is divided into two stages: "Digging pattern" and "Honey picking mode".

Stage 1: "Digging pattern", the mathematical model of this process is as follows:

$$x_{\text{inew}} = x_{\text{prey}} + F.\beta.I.x_{\text{prey}} + F.r_3.\alpha.d_{\text{i}}.|\cos(2\pi r_4).[1-\cos(2\pi r_5)]| \tag{28}$$

Within this, x_{inew} is the updated position of individual $i, \beta \geq 1$, which represents the predation ability of the honey badger and is usually set to 6 , and r_3, r_4, and r_5 are all random numbers between $[0,1]$ that are not the same as each other.

The specific form of the parameter F is as follows:

$$F = \begin{cases} 1, r_6 \leq 0.5 \\ -1, \text{ else} \end{cases} \tag{29}$$

Where, r_6 is a random number between $[0, 0.5]$.

Stage 2: "Honey picking pattern", the mathematical model of this process is as follows:

$$x_{\text{inew}} = x_{\text{prey}} + F \cdot r_7 \cdot \alpha \cdot d_i \tag{30}$$

Within this, r_7 is also a random number between $[0, 1]$.

The process of solving the power system capacity configuration model using HBA is shown in Fig. 4 below.

5. Experiments and analysis

5.1. Experimental parameter setting

Selecting the actual operation data of a regional tram line in one year as the research object for analysis, the main technical parameters of the tram are shown in Table 3 below [23]. In order to fully match the design objectives of low cost and long life of the power system, the hybrid power system uses AMP20M1HD-A lithium iron phosphate battery of A123 company, the fuel cell stack provided by the French Fuel Cell Laboratory (FCLAB), and MAXWELL's BCAP3000 supercapacitor as the energy storage elements. The lithium battery and the supercapacitor are used as the main power source, the fuel cell is used as the auxiliary energy source. The remaining technical parameters are detailed in Appendix A, Table A2 and Table A3. The example analysis considers the effect of different energy storage methods on the average annual minimum cost of the power system.

5.2. HBA Algorithm Validation

According to the HBA optimization algorithm in Section 4.3, the population size N is set to be 50 , the maximum number of iterations T to be 500 , and the problem dimension D to be 30. In order to validate the convergence performance of the HBA algorithm, the single-peak function Sphere and the multiple-peak function Ackley are introduced and the optimal value of these benchmark functions is set to be zero. The convergence of the HBA algorithm on the Sphere function is shown in Fig. 5(a).

As can be seen from Fig. 5(a), HBA converges very rapidly on the Sphere function and the convergence accuracy keeps improving to an exponential level of 10^{-100}. This is due to the fact that in the HBA algorithm, all individuals update their positions according to the prey, that is, the optimal individual in the population, and the population always evolves towards the optimal individual. And the single-peaked function Sphere does not have a local optimum, so the convergence curve of the algorithm is always in a decreasing trend.

The multiple peaks function has the ability to jump out of the local optimum compared to the single peaks function, which can be used to test the performance of the algorithm comprehensively. The convergence curve of the HBA algorithm on the Ackley function is shown in Fig. 5(b). As can be seen in Fig. 5(b), the HBA algorithm evolves rapidly towards the optimal solution on the Ackley function, and the convergence accuracy reaches 10^{-15} exponential levels in less than 50 iterations. In summary, it can be concluded that the HBA algorithm has fast convergence speed, high accuracy and strong search capability, which provides sufficient basis for the capacity allocation results.

5.3. Capacity configuration results

Taking the case of capacity configuration of single-type battery energy storage and hybrid energy storage as an example, using Eq. (25) to initialize the parameters of the algorithm, combining the objective function proposed in section 4.1 and the constraints proposed in section 4.2, and calculating according to the HBA algorithm proposed in section 4.3, the optimal results of the capacity configuration are obtained as shown in Table 4. Table 4 shows that the use of hybrid energy storage increases the rated power and rated capacity of the supercapacitor but also reduces the rated power and rated capacity of the battery.

Comparing the total average annual minimum cost under the two types of energy storage, it can be obtained that the total average annual minimum cost of using single battery energy storage is 23.645 million yuan, while the total average annual minimum cost of using hybrid energy storage with fuel cell and supercapacitor as the auxiliary power source is only 14.603 million yuan, which is a reduction of 38.2% compared with single-type of energy storage, and it reduces the cost and improves the economy to a certain extent.

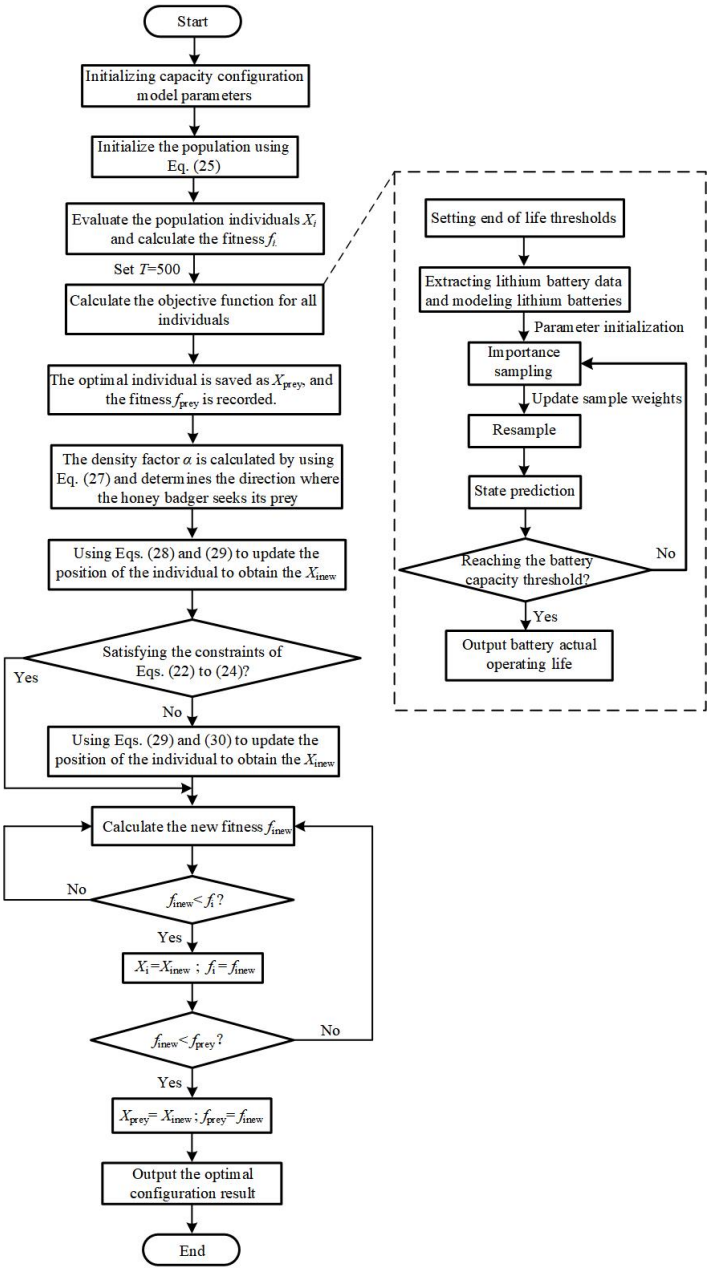

Fig. 4. Capacity configuration flow chart.

Table 3. Main technical parameters of the tram.

Parameters	Value
Drive motor/kW	8×110
Converter/V	DC750(500-900)
Axle weight/t	12
Train weight/t	47
Train body length /m	31075
Mileage /km	> 40
Maximum operating speed /(km/h)	60

5.4. Capacity configuration results comparative analysis

This paper compares the effect of two energy storage methods on the total annual average minimum cost of the power system, and the results show that the use of hybrid energy storage can significantly reduce the cost and improve the

Table 4. Capacity configuration results.

Types		Single-type battery energy storage	Hybrid energy storage
Rated power/MW	Batteries	8.39	3.46
	Supercapacitor	0.00	7.08
Rated capacity/MW · h	Batteries	7.80	4.42
	Supercapacitor	0.00	2.32
Total average annual mini cost/Million Yuan		23.645	14.603

Table 5. Comparison of capacity configuration results.

Types	Total average annual mini cost/Million Yuan
Model 1	2657.71
Model 2	2583.76
Model 3	2379.45
Method of this paper	1460.3

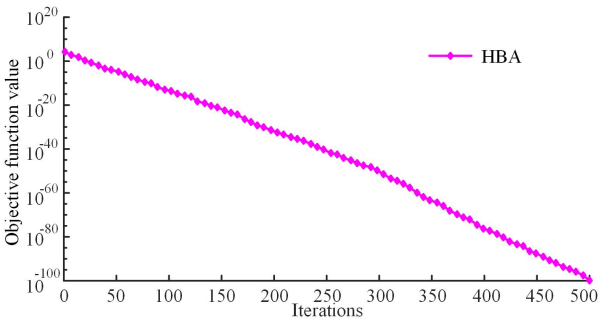

(a) Sphere function.

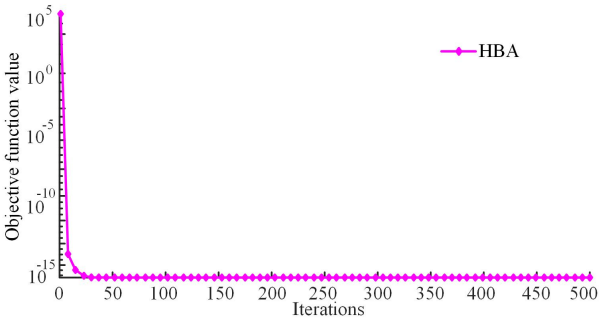

(b) Ackley function.

Fig. 5. Validation function.

system economics. The results of this paper are compared with the existing literature [24] on capacity configuration strategies with the same optimization objective of total annual minimum cost. [24] investigates the configuration results by comparing three energy storage models with the optimization objective of minimizing the annual cost. Model 1: No energy storage device model. Mode 2: Single energy storage device mode. Model 3: Hybrid energy storage device model. The comparison between the capacity configuration results of [24] and this paper is shown in Table 5.

From Table 5, it can be seen that the total annual cost of adopting model 3 in the literature [24] is reduced by 10.5% and 7.9% compared to model 1 and model 2 respectively, which indicates that adopting the hybrid energy storage configuration model is more economical compared to the no storage device model and the single energy storage device model. The hybrid energy storage method used in this paper has a smaller total annual cost compared to Model 3, which verifies the effectiveness and superiority of the configuration method in this paper.

6. Conclusions

1. The particle filtering algorithm can effectively predict the remaining useful life of lithium batteries, and the more prediction cycles the more accurate the remaining life prediction results. Compared with the extended Kalman filter algorithm to predict the remaining life of lithium battery, the prediction error is significantly reduced, and the proposed method has a higher prediction accuracy.

2. Considering the remaining useful life of the lithium battery in the power system capacity configuration model, the remaining useful life prediction of the lithium battery in the early stage provides a prerequisite for the capacity configuration in the later stage, so as to improve the accuracy of the capacity configuration.

3. According to the different periods of generation, this paper divides the cost of the power system into three categories: initial investment cost, component replace-

ment cost, and operation and maintenance cost, which is more practical than the cost calculation method that only considers one-time investment.

4. The use of hybrid energy storage reduces the rated power and rated capacity of the batteries and the total average annual minimum cost is 14.603 million yuan, which is a 38.2% reduction compared to single-type battery energy storage. Hybrid energy storage has both performance and economic advantages over single-type battery energy storage.

The particle filter algorithm adopted in this paper is simple and easy, but the accuracy is not the highest. It can be considered to combine with other prediction methods to find a method that can effectively implement online prediction of the remaining useful life of lithium batteries, and further improve the prediction accuracy, which will become the focus of subsequent research work. But at the same time, online prediction methods also greatly increase the workload and have certain limitations. Due to the differences in the operating data of streetcars under different operating conditions, the capacity configuration of the hybrid system will be affected. Subsequently, different operating conditions will be considered comprehensively and the system capacity configuration method will be studied in a targeted manner to further improve the economy of the system.

Acknowledgements

This work was supported in part by China Railway "14th Five-Year Plan" Science and Technology Major Special Program (2021CXZ021) and Gansu Province Education Department Outstanding Graduate Students "Innovation Star" Program (2023CXZX-616).

nomenclature

Acronyms

AUKF	Unscented Kalman Filtering
EKF	Extended Kalman Filter
FCLAB	Fuel Cell Laboratory
HBA	Honey Badger Algorithm
NASA PCoE	NASA Prognostics Center of Excellence
PF	Particle Filtering
RUL	Remaining Useful Life
SOC	State of Charge

Variables

α	Density factor
$\delta(\bullet)$	A 0-1 variable function
Co_2	Dissolved oxygen concentration at the cathode gas-liquid interface
$h(\cdot)$	Observation equation
$\omega_k^{(i)}$	Particle weights
$\xi_1, \xi_2, \xi_3, \xi_4$	Empirical factors
A b	Amplitude of the index area
a and c	Lithium battery degradation rate
a and c	Lithium battery internal impedance
B	Inverse of the time constant of the index area
B'	System parameter
B_{cell}	Equivalent internal resistance
C	Polarization constant
$C[Q/Q-it]i$	Polarization voltage
$C[Q/Q-it]$	Polarization resistance
C^T	Capacitance value of the supercapacitor composed of N_S monomers in series and N_P monomers in parallel
C_1	Initial investment cost
C_2	Component replacement costs
C_3	Operation and maintenance costs
C_{bat}	Rated capacity of the battery
C_{cap}	Rated capacity of the supercapacitor
C_{min}	Average annual minimum cost
D	Problem dimension
d_i	Distance between the prey and the ith honey badger
E_0	Lithium battery constant voltage
$ENerast$	Thermodynamic electric potential
$f()^*$	State equation
I	Actual current density of the fuel cell
i^*	Filtered lithium battery current
$I_{\max}$	Maximum current density of the fuel cell
isc	Transient current
it	Actual lithium battery charge
k	Number of cycles
lb_j	Lower bound for the jth dimensional variable
m_{bc}	Capacity unit price of the battery
m_{bp}	Power unit price of the battery
m_{cc}	Capacity unit price of the supercapacitor
m_{cp}	Power unit price of the supercapacitor
n_{bat}	The number of times the battery is replaced throughout the operation
n_{cap}	The number of times the supercapacitor is replaced throughout the operation
N_{eff}	Effective number of particles
N_{th}	Particle degradation threshold
O	Odor intensity
P_{bat}	Rated power of the battery
P_{cap}	Rated power of the supercapacitor
P_{ch}	Charging power of the power system
P_{disch}	Discharging power of the power system
Q	Lithium battery capacity
Q^T	Total electric charge
r_1-r_7	Random numbers between [0,1]
R_b	Lithium battery internal resistance
R_{SC}	Equivalent internal resistance
S	Concentration intensity
$SOC_{bat-max}$	Upper limit of state of charge of the battery
$SOC_{bat-min}$	lower limit of state of charge of the battery
$SOC_{cap-max}$	Upper limit of state of charge of the supercapacitor
$SOC_{cap-min}$	lower limit of state of charge of the supercapacitor
T	Internal temperature of the fuel cell
T_{act}	Actual operating life of the power system
t_d	Lithium battery degradation rate
T_{max}	Maximum number of iterations
ta	Time when lithium battery is fully charged
U_{sep}	Concentration polarization overvoltage
u_{bat}	Unit price for operation and maintenance of the battery
u_{cap}	Unit price for operation and maintenance of the supercapacitor
ub_j	Upper bound for the jth dimensional variable
$Uobme$	Ohmic polarization overvoltage
$Uselp$	Fuel cell output voltage
Ust	Activation polarization overvoltage
V_{bati}	Lithium battery terminal voltage
V_{SC}	Supercapacitor output voltage
ve	System noise
wk	Observation noise
x	State value
x_{ij}	The jth dimensional variable for individual i
x_{inew}	Updated position of individual i
x_{prey}	Optimal individuals in the population

y Observed value

References

[1] J. Luo, X. Wei, S. Gao, T. Huang, and D. Li, (2022) *"Summary and Outlook of Capacity Configuration and Energy Management Technology of High-Speed Railway Energy Storage System"* **Proceedings of the CSEE *42***: 7028–7051. DOI: 10.13334/j.0258-8013.pcsee.211526.

[2] K. Zeng, (2014) *"Lithium-ion Battery Life Influence Factor and the Need to Protect"* **Electric Tool**: 12–15. DOI: 10.16629/j.cnki.1674-2796.2014.s1.008.

[3] Y. Zhang, X. Zhang, X. Li, W. Zhang, and F. Zhao, (2024) *"Lithium-ion Battery Life Prediction Based on Extended Kalman Filter"* **Journal of Chongqing University of Technology(Natural Science) *38***: 282–288.

[4] H. Shen, Z. Liu, L. Shao, X. He, Y. Zheng, Z. Liu, and Y. Zhang, (2023) *"State of Charge Estimation of Lithium Battery Based on Improved Unscented Kalman Filter"* **Control Engineering of China *30***: 2217–2225. DOI: 10.14107/j.cnki.kzgc.20220705.

[5] W. Luo, Y. Zhou, and B. Zhang, (2021) *"Target Tracking Based on Particle Filter Under Nonlinear and Non-Gaussian Conditions"* **Foreign Electronic Measurement Technology *40***: 45–51. DOI: 10.19652/j.cnki.femt.2102675.

[6] N. He, S. Zhang, R. Li, F. Gao, and J. Wang, (2024) *"RUL Prediction of Lithium Battery Based on Particle Filter and GRU Neural Network Fusion"* **Journal of Harbin Institute of Technology *56***: 142–151.

[7] D. Jin, Z. Gu, and Z. Zhang, (2023) *"Lithium Battery Health Degree and Residual Life Prediction Algorithm"* **Power System Protection and Control *51***: 122–130. DOI: 10.19783/j.cnki.pspc.211447.

[8] N. Zhang, J. Tang, P. Fayu, and K. Zhou, (2021) *"Method for Predicting Cycle Life of Lithium Iron Phosphate Power Battery"* **Journal of Electronic Measurement and Instrumentation *35***: 33–39. DOI: 10.13382/j.jemi.B2003160.

[9] X. Han, C. Cheng, T. Ji, and H. Ma, (2013) *"Capacity Optimal Modeling of Hybrid Energy Storage Systems Considering Battery Life"* **Proceedings of the CSEE *33***: 91–97+16. DOI: 10.13334/j.0258-8013.pcsee.2013.34.015.

[10] Z. Sun, Y. Liu, J. Hao, T. Wang, and H. Xie, *"Research on Frequency Dynamic Characteristics and Optimization Configuration of Energy Storage Capacity under Fault Disturbance of Wind-Thermal-Storage System"* **Power System Technology**: 1–13. DOI: 10.13335/j.1000-3673.pst.2024.0437.

[11] Q. Lu, Q. Ma, W. Wei, Z. Yu, and Y. Liu, (2022) *"Optimal Configuration of Energy Storage Parameters Based on Confidence Capacity of Wind Farms"* **Transactions of China Electrotechnical Society *37***: 5901–5910. DOI: 10.19595/j.cnki.1000-6753.tces.220939.

[12] M. Guo, Y. Mu, Q. Xiao, H. Jia, X. Yu, and W. He, (2021) *"Optimal configuration of electric/thermal hybrid energy storage for park-level integrated energy system considering battery life loss"* **Automation of Electric Power Systems *45***: 66–75.

[13] Z. Liu, L. Zhang, P. Kou, and S. Zou, (2023) *"Capacity Allocation Optimization on Grid Connected System Consisting of Wind Power, Photovoltaic Power, Pumped Storage and Battery"* **Journal of Chinese Society of Power Engineering *43***: 1151–1159. DOI: 10.19805/j.cnki.jcspe.2023.09.007.

[14] M. Souleman, L. Dessaint, and K. AI-Haddad, (2013) *"A Comparative Study of Energy Management Schemes for A Fuel Cell Hybrid Emergency Power System of Electric Aircraft"* **IEEE Transactions on Industrial Electronics *61***: 1320–1334.

[15] J. Wang, J. Chen, F. Lan, Q. Liu, and C. Zeng, (2023) *"Global Sensitivity Analysis of Multi-scale parameters of the fuel cell model based on two cost functions"* **Automotive Engineering *45***: 393–401. DOI: 10.19562/j.chinasae.qcgc.2023.03.006.

[16] K. Oldham, (2008) *"A Gouy-Chapman-Stern Model of the Double Layer at A (Metal)/(Ionic Liquid) Interface"* **Journal of Electroanalytical Chemistry *613***: 131–138.

[17] T. Xia, Y. Zhang, M. Yang, X. Ji, Z. Yin, and X. Zhang, (2022) *"Robust Forecasting-Aided State Estimation Method of Distribution Network Based on Long-short Term Memory Neural Network and Particle Filter"* **High Voltage Engineering *48***: 1343–1355. DOI: 10.13336/j.1003-6520.hve.20210509.

[18] C. Xu, L. Li, Y. Yang, and K. Wang, (2020) *"Lithium-ion Battery SOH Estimation Based on Improved Particle Filter"* **Energy Storage Science and Technology *9***: 1954–1960. DOI: 10.19799/j.cnki.2095-4239.2020.0159.

[19] Q. Zhang, Z. Zhang, T. Li, and J. Zheng, (2017) *"A Particle Filter with Perturbation for Fault Detection"* **Electric Machines and Control *21***: 103–109. DOI: 10.15938/j.emc.2017.11.014.

[20] P. Wang, Q. Gong, J. Zhang, and Z. Cheng, (2021) *"An Online State of Health Prediction Method for Lithium Batteries Based on Combination of Data-Driven and Empirical Model"* **Transactions of China Electrotechnical Society *36***: 5201–5212. DOI: 10.19595/j.cnki.1000-6753.tces.210385.

[21] G. Lou, W. Lin, and Y. Wang, (2024) *"Remaining Useful Life Prediction of Supercapacitors Based on DMM-EKF"* **Journal of Mechanical Engineering *60***: 306–316.

[22] B. Yang, B. Liu, Y. Chen, S. Wu, H. Shu, and Y. Han, (2024) *"Array Optimization of Wave Energy Converters Via Improved Honey Badger Algorithm"* **Journal of Shanghai Jiaotong University *58***: 1465–1478. DOI: 10.16183/j.cnki.jsjtu.2023.030.

[23] F. Gao, Y. Qiang, Z. Gao, H. Xu, and Z. Shi, *"Combined Online and Offline Control for Fuel Cell Tram Energy Management Strategy"* **Journal of Jilin University (Engineering and Technology Edition)**: 1–13. DOI: 10.13229/j.cnki.jdxbgxb.20221593.

[24] Y. Wang, F. Song, Y. Ma, Y. Zhang, J. Yang, Y. Liu, F. Zhang, and J. Zhu, (2020) *"Research on Capacity Planning and Optimization of Regional Integrated Energy System Based on Hybrid Energy Storage System"* **Applied Thermal Engineering *180***: 115834.